A Macroscopic Model of Oscillation in Ensembles of Inhibitory and Excitatory Neurons [1]

Joydeep Ghosh [2]
Hung-Jen Chang
Kadir Liano

Department of Electrical and Computer Engineering
The University of Texas at Austin
Austin, TX 78712

Contents

1 Introduction **1**

2 A Macroscopic Model for Cell Assemblies **3**
2.1 Description of Individual Cells 3
2.2 Characterization of Cell Assemblies 5

3 Interactions Between Two Neural Groups **8**

4 Stability of Equilibrium States **13**

5 Oscillation Frequency Estimation **15**

6 Experimental Validation **18**

7 Conclusion **22**

[1] Supported by an NSF grant MIP-9011787 and by ONR contracts N00014-89-C-0298 and N00014-92-C-0232.

[2] Please contact *ghosh@pine.ece.utexas.edu and hjchang@pine.ece.utexas.edu* for any questions or comments regarding this paper, or for reprint requests.

List of Figures

1 Microscopic model of a neural cell 4
2 (a) Microscopic transfer function, (b) Macroscopic transfer function 7
3 Interactions between excitatory and inhibitory neuronal assemblies. . 8
4 Generic graph of $f_P = 0$ with a single root. 11
5 Generic graphs of $f_P = 0$ with three roots. 11
6 Generic graph of $f_N = 0$. 12
7 Phase plot of all three possible solutions. 15
8 Periodic solution. 19
9 Spiral to periodic solution. 20
10 Fixed point solution. 21

Abstract—*Very large networks of neurons can be characterized in a tractable and meaningful way by considering the average or ensemble behavior of groups of cells. This paper develops a mathematical model to characterize a homogeneous neural group at a macroscopic level, given a microscopic description of individual cells. This model is then used to study the interaction between two neuron groups. Conditions that lead to oscillatory behavior in both excitatory and inhibitory groups of cells are determined. Using Fourier series analysis, we obtain approximate expressions for the frequency of oscillations of the average input and output activities, and quantitatively relate them to other network parameters. Computer simulation results show these frequency estimations to be quite accurate.*

Keywords—Large neural networks, Ensemble behavior, Oscillations, Inhibitory and Excitatory Cell Assemblies, Frequency estimation.

1 Introduction

Biological neural networks consist of very large numbers of neurons. The human brain has over 10^{11} neurons, with an average connectivity in the thousands. Faced with numbers of this magnitude, it is impossible and meaningless to model every single neuron and its interactions with the entire system. To gain insight into the complex functions performed by neural systems, an understanding of the overall network in terms of ensemble or group behavior and group interaction is required that is not overwhelmed by the details of individual neurons [Ama72, Ede87]. Such macroscopic models are useful in studying collective behavior of biological neural systems, and in particular, macroscopic oscillations in cell assemblies.

Oscillatory phenomena have been widely observed in cortical circuits at similar frequencies (in the 35-60 Hz range) and at many different spatial scales. They occur in single neurons, within small (10-100 cell) neural networks, and in large (over 10K cells) networks. Oscillations are considered fundamental to memory storage and temporal association functions in biological organisms [Bow90, vB86, Pav73].

Large-scale rhythmic/oscillatory phenomena is integral to the dynamic timing mechanisms for heart beat, EEG waves, breathing, walking, and other activities. Recent experiments by Gray and Singer [GS89] and by Traub, Miles, and Wong [TMW89], among others, show oscillations occurring at the level of local population of cortical neurons. Rhythmic patterns emerge even though single neurons may fire asynchronously. Some of the remarkable characteristics of cortical oscillations is the synchronization of oscillations between spatially disparate cell assemblies, and of phase locking [AB89, GS89]. Such experiments, together with previous theoretical investigations [vB86], give credence to the labeling hypothesis, wherein cell assemblies are established through oscillations and labeled by their phase and/or frequency. The labeling hypothesis postulates that neural information processing

is intimately related to the temporal relationships between the labels of different populations.

To study and characterize the behavior of large populations of neurons, several researchers have developed macroscopic models that characterize the aggregate population behavior, in a way similar to how statistical mechanics has been used to obtain global quantities like pressure and temperature starting from molecular level description of gasses. Pioneering research in developing macroscopic models of large neural ensembles has been performed by Amari, who studied characteristics of random networks of threshold logic elements (Mc Culloch-Pitts formal neurons) [Ama71], and subsequently, of continuous time analog neurons [Ama72]. The weights and thresholds in these networks were random variables, and did not change as the ensemble evolved, i.e., no learning mechanisms were investigated. Using some simplifying assumptions including the stochastic independence among cell membrane potentials, Amari showed that a homogeneous random net is monostable or bistable. Moreover, oscillations could emerge from the interactions between two random nets consisting of excitatory and inhibitory classes of elements respectively. At about the same time, Wilson and Cowan [WC72] showned the presence of oscillations in coupled subpopulations of inhibitory and excitatory neurons with refractory periods, but with non-adaptive weights. Amari's results were later expressed in rigorous mathematical framework by Geman [Gem82]. Similarly, Wilson and Cowan's system has been further analyzed by other researchers [Som88] and oscillator models have been developed for specific circuits such as the visual cortex [SW90].

Notable among recent research along these lines is the work by Atiya and Baldi [AB89], who consider interacting cell assemblies of continuous time analog neurons as well as "integrate-and-fire" type of neurons. If the assemblies are arranged in layers, with feedback from the top-most to the bottom-most layer (thus resulting in a ring structure), and the number of inhibitory layers are odd, then oscillations arise easily if the cell gains are high enough. Also, provided the cell time constants are very similar within a layer, all the cells belonging to that layer tend to phase lock in a few time constants. As before, learning mechanisms are not incorporated in their framework.

An alternative approach to obtaining oscillatory phenomena in neural networks is to use a more involved model of the individual cells that results in these cells becoming non-linear neuronal oscillators by themselves. For example, Kammen, Koch, and Holmes [KKH90] assume a population of neuronal oscillators firing repetitively in response to synaptic input which is purely excitatory. They investigate two basic neuronal network architectures, namely, the linear chain model and comparator model, that incorporate either nearest neighbor or global feedback interactions. They conclude that non-local feedback plays a fundamental role in the initial synchronization and dynamic stability of the oscillations. Baird [Bai90] discusses a generic model of oscillating cortex which assumes a minimal coupling structure.

The network has explicit excitatory neurons with local inhibitory interneuron feedback that form a set of nonlinear oscillators coupled only by long range excitatory connections. He argues that an oscillatory associative memory function can be realized in such a system by using a local Hebb-like learning rule. Due to the complex characterization of individual cells, it is difficult to obtain a useful macroscopic description using such approaches.

In [CGL92], authors have presented a macroscopic model for a homogeneous cell assembly, wherein each individual cell is an analog neuron whose characteristics are given by a well known model [Hop84]. This model is distinguished from previous work by the fact that it relates in quite some detail the macroscopic variables to biologically motivated cell parameters, and even more so by the incorporation of adaptive weight dynamics. The latter factor makes it possible to achieve rhythmic patterns in ensemble activity even in an isolated homogeneous cell assembly with no external periodic inputs. The model not only predicts such situations, but is also able to estimate the frequency of oscillation and indicate how the parameters could be changed to obtain a desired oscillation frequency.

Here, we apply a model similar to that developed in [CGL92] to study the interaction of excitatory and inhibitory neuron groups. For simplicity, the weights are not adapted, though this possibility is kept open for future research. The main contribution of this report is to quantify the situations that lead to stable macroscopic behavior, and to estimate the oscillation frequencies. The frequency estimates are observed through simulations to be quite accurate. We begin in the next section by summarizing the macroscopic model. Section 3 applies this model to analyze a system with inhibitory and excitatory neurons. Stability analysis of this system is performed in Section 4, and the frequency of oscillation is estimated in Section 5 using a first-order approximation. Simulation results presented in Section 6 support the mathematical analysis given in previous sections.

2 A Macroscopic Model for Cell Assemblies

2.1 Description of Individual Cells

Macroscopic model for neuronal assemblies depend on the characterization of individual neurons as well as on the network architecture that defines how these neurons interact with one another. The model of individual neurons should be biologically plausible without incorporating details that do not significantly affect macroscopic behavior such as ensemble oscillations. These cells should at least be able to integrate information over time. Thus connectionist-type cells, where the instantaneous output is a linear or sigmoidal function of a weighted sum of inputs at that instant, are too simplistic and clearly inadequate.

The next level of complexity is to model a set of n asynchronous cells by n coupled first-order differential equations. A popular generic form is [Cow67, Ama72,

GC83, Hop84]:

$$\frac{du_i}{dt} = -\frac{u_i}{\tau_i} + \sum_{k=1}^{n} w_{ik} g_k(u_k) + h_i, \quad 1 \leq i \leq n, \tag{1}$$

where u_i is the internal state of the ith neuron, and represents the short-time averaged value of the membrane potential, τ_i is a time constant, w_{ik} represents the weight or synaptic strength from neuron k to i, h_i is a threshold, and $g_k(\cdot)$ is the input-output "squashing" cell-activation function for the kth neuron. The output can be interpreted as the mean firing rate of the neuron. This system can converge to equilibrium points if the weights are symmetric [GC83, Hop84], if all weights are positive [Hir89], or if the weights and thresholds are independent, normally distributed random variables [Ama72]. However, oscillatory behavior has not been established for this system.

While the model given by Eq. (1) does not capture many features of biological neurons, it is quite popular because of its simple nature and because it is easily amenable to hardware implementation [Hop84]. Further detail can be added by considering "integrate and fire" type of neurons [AB89], by applying cable theory, or by using compartmental models [KS89]. However, such detailed modeling is found to be an overkill when considering large systems of neurons.

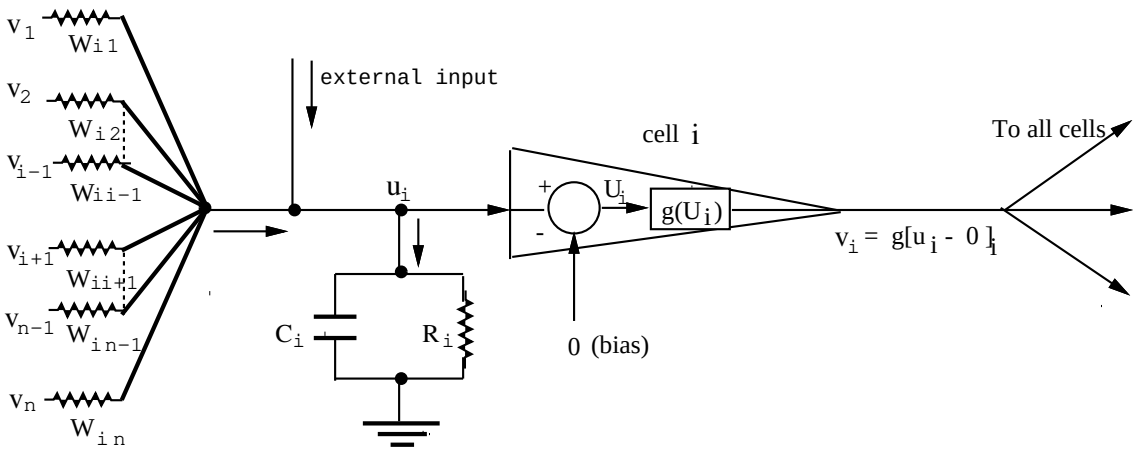

Figure 1: Microscopic model of a neural cell

In this article, we use a Hopfield-type neural model, a form of Eq. (1) in which each cell is represented by an electrical circuit as depicted in Figure 1. The synaptic strength from cell k to cell i is denoted by a conductance $W_{ik}(t)$, and R_i, C_i are the cell membrane resistance and capacitance of cell i. Let θ_i be the threshold for neuron i to fire, $U_i(t) = u_i - \theta_i$ the effective membrane potential, a_i the cell time constant, $T_{ik} = \frac{W_{ik}}{C_i}$ the effective connection strength from cell k to cell i, $I_i(t)$ the effective external current into cell i, and v_i(t) the cell output which can be considered as a

short time average of its firing rate. By applying Kirchoff's current law to the cell input and simple algebraic manipulation, one obtains:

$$\frac{dU_i(t)}{dt} = -\left(a_i U_i(t) + \theta_i\right) + \sum_{k=1}^{n} T_{ik}(t) v_k(t) + \frac{I_i(t)}{C_i}. \tag{2}$$

The model may also include a formula for weight adaptation. In this paper, we acknowledge that the weights could be time-varying without explicitly using this fact.

A popular choice for the input-output transfer function for individual cells is:

$$\begin{aligned} v_i(t) &= \frac{1}{1 + e^{-2\lambda U_i(t)}} \\ &\triangleq g[U_i(t)]. \end{aligned} \tag{3}$$

Eq. (2) and Eq. (3) thus characterize the microscopic model.

We note that the output of a neuron is a train of action potentials or spikes propagated through its axon. An action potential occurs when the membrane potential reaches a particular threshold. At that juncture, the membrane potential is "discharged" to a resting value, and the neuron is prevented from firing for a short refractory period after which the membrane potential can charge up again. While several detailed models exist for this input-output behavior, it is deemed sufficient to model the neuron as having a continuous output voltage v_i that is a function of the input voltage u_i at the same instant, for the purposes of studying macroscopic phenomena. If the refractory period is sufficiently smaller than the interval between successive firings, then $v_i(t)$ can be interpreted as the short-term average firing rate of the ith neuron [Ami89] and be obtained by a smooth function such as in Eq. (2).

2.2 Characterization of Cell Assemblies

Several researchers have studied the properties of large neural networks by aggregating them into interacting groups or clusters [Ama72, Ede87, Ama90, CG93]. Typically a group exhibits more homogeneity among its constituent neurons, has higher internal connectivity, and/or is used to represent a particular hypothesis [GH89]. Well known examples include the neuronal groups of Edelman [Ede87], and the neural clusters used for distortion invariant pattern matching by von der Malsburg [vdM88]. In this section, we apply methods in statistics to build a macroscopic neural model.

Macroscopically, the behavior of a cell assembly can be characterized in terms of the time or ensemble averaged behavior of the homogeneous collection of neurons that populate it. For large assemblies, we can consider an individual cell parameter $x_i(t)$ as an instance of a ***random process***, $x(t)$. Thus, for any specific time instant t, $x(t)$ is a random variable. The corresponding ***system-level*** parameter of interest is

the sample mean, $\bar{x}(t)$, or the expectation, $\langle x(t) \rangle$. A macroscopic model reduces the system description from a set of $2n$ coupled equations to a few equations involving expectations and standard deviations of these random variables.

The Law of Large Numbers shows that the expectation approaches the sample average for large n. In the derivations below, the expectation and sample average are interchangeable, i.e.,

$$\bar{x} \triangleq \frac{1}{n} \sum_{i=1}^{n} x_i \approx \langle x \rangle .$$

Also, by definition,

$$\frac{d\overline{x}(t)}{dt} = \frac{d}{dt} \left[\frac{1}{n} \sum_{i=1}^{n} x_i(t) \right] = \frac{1}{n} \sum_{i=1}^{n} \frac{dx_i(t)}{dt} = \overline{\frac{dx_i(t)}{dt}}. \tag{4}$$

By applying Eq. (4) to Eq. (2), we obtain:

$$\frac{d\overline{U}(t)}{dt} = -\overline{aU(t)} + -\overline{a\Theta(t)} + \overline{T(t)v(t)}, \tag{5}$$

where

$$\Theta_i(t) = \theta_i - R_i I_i(t)$$

and

$$T_i(t) = \sum_{k=1}^{n} T_{ki}(t).$$

At first glance, the macroscopic Eq. (5) seems intractable because of the coupled parameters. Fortunately, it seems that when n is large, a knowledge of any one of the random variables would contribute very little information about the other random variables [Gem82]. Based on this insight, Amari introduced the concept of a symmetric, random net to describe networks composed of one homogeneous class of analog elements described by Eq. (1), in which all the weights, $T_{i,j}$ are independent, identically distributed (i.i.d.) random variables. The thresholds are also i.i.d.s but subject to a probability distribution different from that for the weights. For such systems, a "local chaos" hypothesis analogous to the one widely used in statistical mechanics, has been proposed. This hypothesis assumes that the solutions of individual equations (in our case, Eq. (2)) within the system are mutually independent. The chaos hypothesis was originally postulated by Rozonoer [Roz69]. Since then, it has been supported by mathematical analysis and by simulations on large systems of randomly coupled equations [Ama72, Gem82], and is key to the development of an elegant macroscopic model of cell assemblies.

For our more detailed model of Eq. (2), the comments made above provide a natural definition of a cell assembly to be a symmetric, random network of homogeneous neurons. This implies that the parameters $a_i, C_i^{-1}, T_i(t), U_i(t), I_i(t)$ and θ_i are from independent distributions at any given time instant, t. The output, $v_i(t)$

of course depends on $U_i(t)$, but is independent of the other parameters. For such a system, the coupled parameters $(a_i, U_i), (a_i, \Theta_i), (T_i, v_i)$ in Eqs. (5) can be separated to yield:

$$\frac{d\overline{U}(t)}{dt} = -\overline{a}\overline{U}(t) - \overline{a}\overline{\Theta}(t) + \overline{T}(t)\overline{v}(t). \tag{6}$$

As presented in [CGL92], we know that the standard deviation of U_i, $\sigma_U(t)$ approaches some constant, σ, as $t \to \infty$ $\left(\sigma_U^2(t) \triangleq \langle U - \langle U \rangle \rangle^2 \approx \frac{1}{n}\sum_{i=1}^{n}\left(U_i - \overline{U}\right)^2\right)$, and $U_i(t)$ becomes a linear combination of R_i and θ_i, as $t \to \infty$. Thus, if R_i and θ_i are normally distributed, then $U_i(t)$ is also normally distributed. The average output can then be computed by:

$$\begin{aligned} \overline{v}(t) &= \int_{-\infty}^{\infty} \frac{1}{\sigma\sqrt{2\pi}} \left(\frac{1}{1+e^{-2\lambda U_i}}\right) e^{-\frac{(U_i - \langle U \rangle)^2}{2\sigma^2}} dU_i \\ &\triangleq \overline{g}\left[\overline{U}(t)\right]. \end{aligned} \tag{7}$$

Through the macroscopic transfer function, $\overline{g}(\cdot)$, seems very complex as compared to the sigmoidal microscopic transfer function, $g(\cdot)$, relating the output of a single neuron to its input, it turns out that these two functions have a similar shape as shown in Figure 2. In particular, we can prove that $\overline{g}(\cdot)$ is monotonically increas-

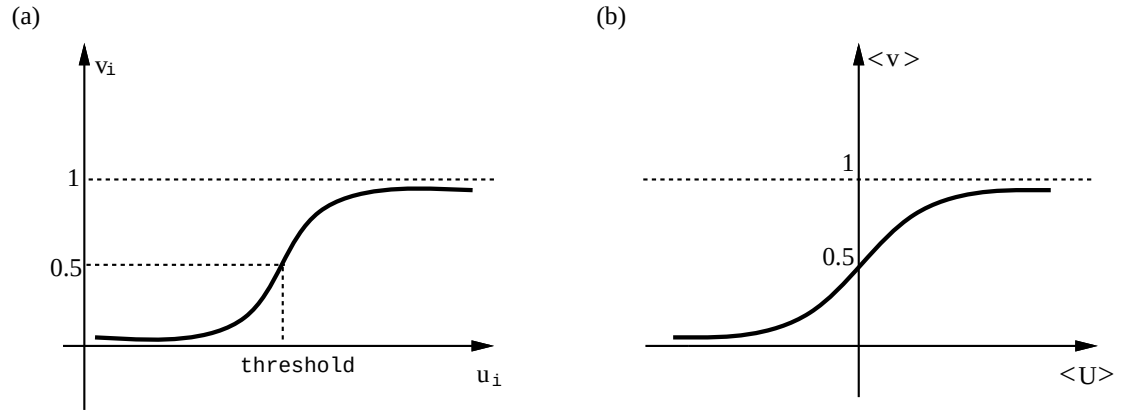

Figure 2: (a) Microscopic transfer function, (b) Macroscopic transfer function

ing by showing the properties of the macroscopic input-output transfer relation that the first derivative of $\overline{g}(\cdot)$ is always positive [CGL92], with

$$\begin{aligned} 0 < \overline{g}(\overline{U}) < 1; \\ \overline{g}(\overline{U}) + \overline{g}(-\overline{U}) = 1; \\ 0 < \overline{g}'(\overline{U}) \leq \frac{1}{\eta}\sqrt{\frac{1}{2\pi}}. \end{aligned} \tag{8}$$

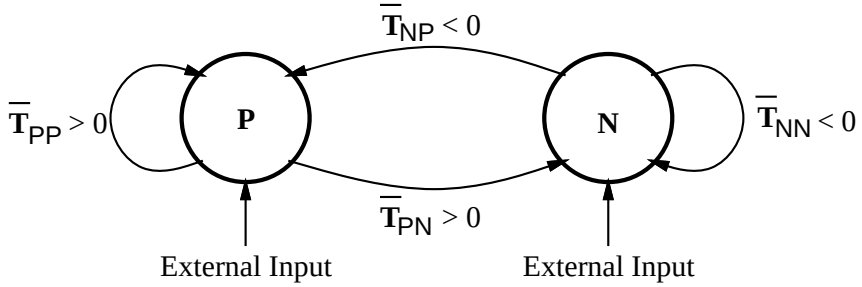

Figure 3: Interactions between excitatory and inhibitory neuronal assemblies.

The above discussion has been mathematically justified in [CGL92], and can be summarized in the following lemma:

Lemma 1 *The shape of the sigmoidal microscopic transfer function* $g[U_i(t)] = \frac{1}{1+e^{-2\lambda U_i(t)}}$ *is conserved by the macroscopic transfer function* $\overline{g}\left[\overline{U}(t)\right]$ *of a large homogeneous population of Hopfield-type neurons, as* $t \to \infty$.

3 Interactions Between Two Neural Groups

In this section, we use the macroscopic state equation of a neuron population derived in the previous section to study a simple model involving the interactions between two groups of neurons, as shown in Figure 3. The P population consists of excitatory neurons and the N population consists of inhibitory neurons. We discuss the qualitative behavior of the equilibrium states of both the excitatory and inhibitory neurons. The equilibrium points of the system are obtained by combining the equilibrium curves of both excitatory and inhibitory neuron populations. These curves also determine the number of fixed points in the system.

The connections between the two neuron groups as shown in Figure 3, as well as other notations used in this section are defined below.

$$\begin{aligned}
\overline{T_{PP}}(t) &= \frac{1}{n_{_P}} \sum_{k=1}^{n_P} \left[\sum_{i=1}^{n_P} T_{PP_{ik}}(t) \right] > 0 \\
\overline{T_{PN}}(t) &= \frac{1}{n_{_P}} \sum_{k=1}^{n_N} \left[\sum_{i=1}^{n_P} T_{PN_{ik}}(t) \right] < 0 \\
\overline{T_{NP}}(t) &= \frac{1}{n_{_N}} \sum_{k=1}^{n_P} \left[\sum_{i=1}^{n_N} T_{NP_{ik}}(t) \right] > 0 \\
\overline{T_{NN}}(t) &= \frac{1}{n_{_N}} \sum_{k=1}^{n_N} \left[\sum_{i=1}^{n_N} T_{NN_{ik}}(t) \right] < 0
\end{aligned}$$

$$
\begin{aligned}
\overline{a_{_P}} &= \frac{1}{n_{_P}} \sum_{i=1}^{n_{_P}} a_{_{P_i}} \\
\overline{a_{_N}} &= \frac{1}{n_{_N}} \sum_{i=1}^{n_{_N}} a_{_{N_i}} \\
\overline{\Theta_P}(t) &= \frac{1}{n_{_P}} \sum_{i=1}^{n_{_P}} \Theta_{P_i}(t) \\
\overline{\Theta_N}(t) &= \frac{1}{n_{_N}} \sum_{i=1}^{n_{_N}} \Theta_{N_i}(t) \\
\overline{U_P}(t) &= \frac{1}{n_{_P}} \sum_{i=1}^{n_{_P}} U_{P_i} \\
\overline{U_N}(t) &= \frac{1}{n_{_N}} \sum_{i=1}^{n_{_N}} U_{N_i} \\
\overline{v_{_P}}(t) &= \overline{g}\left[\overline{U_P}(t)\right] \\
\overline{v_{_N}}(t) &= \overline{g}\left[\overline{U_N}(t)\right] \\
\overline{g}'\left[\overline{U_P}(t)\right] &= \frac{d\overline{v_{_P}}(t)}{d\overline{U_P}(t)} \\
\overline{g}'\left[\overline{U_N}(t)\right] &= \frac{d\overline{v_{_N}}(t)}{d\overline{U_N}(t)}.
\end{aligned}
$$

Assuming that the number of excitatory neurons is close to the number of inhibitory neurons, i.e. $n_{_P} \approx n_{_N}$, the coupled differential equations describing the macroscopic behavior of the system can be derived from equation (6):

$$
\begin{aligned}
\frac{d\overline{U_P}(t)}{dt} &= -\overline{a_{_P}}\,\overline{U_P}(t) - \overline{a_{_P}}\,\overline{\Theta_P}(t) + \overline{T_{PP}}(t)\,\overline{v_{_P}}(t) + \overline{T_{PN}}(t)\,\overline{v_{_N}}(t) \qquad (9) \\
&\triangleq f_{_P}\left(\overline{U_P}(t), \overline{U_N}(t), t\right); \\
\frac{d\overline{U_N}(t)}{dt} &= -\overline{a_{_N}}\,\overline{U_N}(t) - \overline{a_{_N}}\,\overline{\Theta_N}(t) + \overline{T_{NN}}(t)\,\overline{v_{_N}}(t) + \overline{T_{NP}}(t)\,\overline{v_{_P}}(t) \qquad (10) \\
&\triangleq f_{_N}\left(\overline{U_P}(t), \overline{U_N}(t), t\right).
\end{aligned}
$$

The system is in equilibrium when both $f_{_P}$ and $f_{_N}$ are equal to zero after time t is greater than some finite t_0. This means that the system stays in a stationary state $\overline{U_P}(t) = A$ and $\overline{U_N}(t) = B$ for all $t \geq t_0$. The equilibrium point can be shown graphically by plotting the curves $f_{_P} = 0$ and $f_{_N} = 0$ on the $(\overline{U_P}, \overline{U_N})$ plane. Intersections of the two curves specify the equilibrium points of the system. In this paper, we assume that the aggregate values of effective synaptic strengths $\overline{T_{PP}}$, $\overline{T_{PN}}$, $\overline{T_{NP}}$, and $\overline{T_{NN}}$, as well as effective biases $\overline{\Theta_P}$ and $\overline{\Theta_N}$ asymptotically reach constant values. Under this assumption, the equilibrium states may exist because

the intersections then become time-invariant. The assumption is trivially valid if there is no learning and if the average external forcing function is constant. Also, large groups of neurons with self-regulatory mechanisms are expected to exhibit such behavior [Ede87].

The following paragraphs describe the features of the two curves at equilibrium. We start off by analyzing the curve $f_{_P} = 0$. For convenience, let us define

$$h_{_P}(\overline{U_P}(t)) = -\overline{a_{_P}}\ \overline{U_P}(t) - \overline{a_{_P}}\ \overline{\Theta_P} + \overline{T_{PP}}\ \overline{g}(\overline{U_P}(t)). \tag{11}$$

Then,

$$h'_{_P}(\overline{U_P}(t)) = -\overline{a_{_P}} + \overline{T_{PP}}\ \overline{g}'(\overline{U_P}(t)). \tag{12}$$

By equation (8) we have

$$\frac{\overline{T_{PP}}}{\overline{a_{_P}}}\sqrt{\frac{2}{\pi}}\ q(\lambda, \eta_{_P}) \leq 1 \quad \Longleftrightarrow \quad h'_{_P}\left(\overline{U_P}(t)\right) \leq 0 \quad \text{for all } \overline{U_P}(t), \tag{13}$$

where

$$q(\lambda, \eta) \triangleq \frac{1}{\eta}\int_0^\infty \frac{\sinh(2\sqrt{2}\,\lambda\eta y)e^{-y^2}}{1+\cosh(2\sqrt{2}\,\lambda\eta y)}\, y\ dy.$$

Also $h\left(\overline{U_P}(t)\right)$ is continuous and changes from $-\infty$ to $+\infty$ as $\overline{U_P}(t)$ varies from $+\infty$ to $-\infty$. Thus $h\left(\overline{U_P}(t)\right)$ is monotonically decreasing. From equation (9) at equilibrium,

$$f_{_P}\left(\overline{U_P}(t), \overline{U_N}(t), t\right) = 0 \quad \Longleftrightarrow \quad \overline{g}\left(\overline{U_N}(t)\right) = -\frac{1}{\overline{T_{PN}}}\ h_{_P}\left(\overline{U_P}(t)\right),$$

which means that $\overline{g}\left(\overline{U_N}(t)\right)$ is strictly monotonically increasing. From the above discussion, it can be concluded that the relation between $\overline{U_P}(t)$ and $\overline{U_N}(t)$ is monotonically decreasing. Moreover, $0 < \overline{g}\left(\overline{U_N}(t)\right) < 1$ and $h_{_P}\left(\overline{U_P}(t)\right)$ is not bounded, the curve $f_{_P} = 0$ is bounded on $\overline{U_P}$ but not on $\overline{U_N}$. Figure 4 shows the graph $f_{_P} = 0$ satisfying (13).

When (13) is not satisfied, i.e. $\frac{\overline{T_{PP}}}{\overline{a_{_P}}}\sqrt{\frac{2}{\pi}}\ q(\lambda, \eta_{_P}) > 1$, $h_{_P}\left(\overline{U_P}(t)\right)$ may not always be monotonically decreasing. Since $h'_{_P}\left(\overline{U_P}(t)\right)$ is a unimodal function, $h_{_P}\left(\overline{U_P}(t)\right)$ can not have more than three roots. If $\overline{U_{P+}}$ and $\overline{U_{P-}}$ stand for the local maximum and minimum of $h_{_P}\left(\overline{U_P}(t)\right)$, then by (8), $\overline{g}'\left(\overline{U_P}(t)\right)$ is symmetric with respect to the origin. So

$$\overline{U_{P+}} = \left|\overline{g}'^{-1}\left(\frac{\overline{a_{_P}}}{\overline{T_{PP}}}\right)\right| \quad \textit{and} \quad \overline{U_{P-}} = -\left|\overline{g}'^{-1}\left(\frac{\overline{a_{_P}}}{\overline{T_{PP}}}\right)\right|.$$

From the above discussion, it is clear that $h_{_P}\left(\overline{U_P}(t)\right)$ is monotonically increasing over the interval $\left[\overline{U_{P-}}, \overline{U_{P+}}\right]$ and monotonically decreasing outside this interval.

Figure 4: Generic graph of $f_P = 0$ with a single root.

Figure 5: Generic graphs of $f_P = 0$ with three roots.

Figure 6: Generic graph of $f_{_N} = 0$.

Since $0 < \overline{g}\left(\overline{U_N}(t)\right) < 1$, the curve $f_{_P} = 0$ is defined only for $h_{_P}\left(\overline{U_P}(t)\right)$ that satisfies

$$0 < h_{_P}\left(\overline{U_P}(t)\right) < -\overline{T_{PN}}. \tag{14}$$

As $\overline{U_P}(t)$ tends to the bounds of (14), $\overline{U_N}(t)$ tends to infinity. The two conditions that determine the shape of the curve $f_{_P} = 0$ are listed below:

$$0 < h_{_P}\left(\overline{U_{P+}}\right) < -\overline{T_{PN}} \tag{15}$$

$$0 < h_{_P}\left(\overline{U_{P-}}\right) < -\overline{T_{PN}} \tag{16}$$

If both conditions above are satisfied, the curves $f_{_P} = 0$ is shown in Figure 5(a). It has the general shape shown in Figure 5(b) if equation (15) is not satisfied, and Figure 5(c) if equation (16) is not satisfied. However if both conditions are not satisfied, then the general shape of curve $f_{_P} = 0$ is shown in Figure 5(d).

For the curve $f_{_N} = 0$, equation (10) can be written as

$$\overline{g}\left(\overline{U_P}(t)\right) = -\frac{1}{\overline{T_{NP}}}\, h\left(\overline{U_N}(t)\right), \tag{17}$$

where

$$h_{_N}(\overline{U_N}(t)) = -\overline{a_{_N}}\,\overline{U_N}(t) - \overline{a_{_N}}\,\overline{\Theta_N} + \overline{T_{NN}}\,\overline{g}(\overline{U_N}(t)). \tag{18}$$

Since $\bar{g}\left(\overline{U_P}(t)\right)$ increases monotonically and $h_{_N}(\overline{U_N}(t))$ decreases monotonically, equation (18) denotes the monotonically increasing relation between $\overline{U_P}(t)$ and $\overline{U_N}(t)$. Moreover, since $0 < \bar{g}\left(\overline{U_P}(t)\right) < 1$, and $h_{_N}(\overline{U_N}(t))$ is not bounded, the curve $f_{_N} = 0$ is bounded on $\overline{U_N}(t)$ but not on $\overline{U_P}(t)$, as shown in Figure 6. We conclude this section with the following lemma:

Lemma 2 *For a system of coupled excitatory and inhibitory cell assemblies governed by equations (9) and (10), there exists at least one and at most five equilibrium points (except for degenerate cases).*

Notice that the equilibrium of the system is shown graphically by the intersection of the curves $f_{\overline{P}} = 0$ and $f_{\overline{N}} = 0$. The lemma can then be easily proved by intersecting Figure 6 with either Figure 4 or 5.

4 Stability of Equilibrium States

In this section, the stability of equilibrium states is studied using Liapunov's theorem. We then apply Poincaré-Bendixson theorem along with Dulac's criterion [AVK66] to analyze the system defined in Section 3.

In previous section, we showed that there exists at least one fixed equilibrium point, and assumed that $\overline{T}$'s and $\overline{\Theta}$'s become constant. From Liapunov's stability theorem on differential equations [AVK66], the stability of an equilibrium state (A,B) of the system described by equations (9) and (10) can be tested by the matrix

$$M = \left(\begin{array}{cc} \frac{\partial f_{\overline{P}}}{\partial \overline{U_P}} & \frac{\partial f_{\overline{P}}}{\partial \overline{U_N}} \\ \frac{\partial f_{\overline{N}}}{\partial \overline{U_P}} & \frac{\partial f_{\overline{N}}}{\partial \overline{U_N}} \end{array} \right) \Bigg|_{\text{evaluated at (A,B).}} \tag{19}$$

If determinant of M is positive and trace of M is negative then the equilibrium state is stable; it is unstable otherwise. Combining equations (9), (10), and (19),

$$M = \left(\begin{array}{cc} -\overline{a_{\overline{P}}} + \overline{g}'\left(\overline{U_P}(t)\right)\overline{T_{PP}} & \overline{g}'\left(\overline{U_N}(t)\right)\overline{T_{PN}} \\ \overline{g}'\left(\overline{U_P}(t)\right)\overline{T_{NP}} & -\overline{a_{\overline{N}}} + \overline{g}'\left(\overline{U_N}(t)\right)\overline{T_{NN}} \end{array} \right). \tag{20}$$

By condition (8) and the definitions given in the beginning of Section 3,

$$\begin{array}{rcl} \frac{\partial f_{\overline{P}}}{\partial \overline{U_N}} < 0 \quad \text{and} \quad \frac{\partial f_{\overline{N}}}{\partial \overline{U_N}}, < 0; & & \\ det(M) > 0 & \Longrightarrow & \frac{-\frac{\partial f_{\overline{P}}}{\partial \overline{U_P}}}{\frac{\partial f_{\overline{P}}}{\partial \overline{U_N}}} < \frac{-\frac{\partial f_{\overline{N}}}{\partial \overline{U_P}}}{\frac{\partial f_{\overline{N}}}{\partial \overline{U_N}}}. \end{array}$$

If we denote the slopes of curve $f_{\overline{P}} = 0$ and $f_{\overline{N}} = 0$ by S_P and S_N respectively, then

$$det(M) > 0 \quad \Longleftrightarrow \quad S_P\left(\overline{U_P}(t), \overline{U_N}(t)\right) < S_N\left(\overline{U_P}(t), \overline{U_N}(t)\right).$$

The above discussion can be summarized in the following theorem.

Theorem 1 *The equilibrium state (A,B) of the system described by equations (9) and (10) is stable when both conditions below hold, and is unstable otherwise.*

$$S_P(A,B) < S_N(A,B) \quad (det(M) > 0). \tag{21}$$

$$\overline{g}'(A)\overline{T_{PP}} + \overline{g}'(B)\overline{T_{NN}} < \overline{a_{\overline{P}}} + \overline{a_{\overline{N}}} \quad (trace(M) < 0). \tag{22}$$

To discuss the general behavior of our system governed by equations (9) and (10), let us consider a region bounded by a circle:

$$\Re \triangleq \left(\overline{U_P} - A\right)^2 + \left(\overline{U_N} - B\right)^2.$$

We have

$$\begin{aligned}
\frac{d\Re}{dt} &= 2\left[-\overline{a_P}\left(\overline{U_P} - A\right)\overline{U_P} - \overline{a_N}\left(\overline{U_N} - B\right)\overline{U_N}\right] \\
&+ \left[\overline{T_{PP}}\,\overline{g}\left(\overline{U_P}\right) + \overline{T_{PN}}\,\overline{g}\left(\overline{U_N}\right) - \overline{a_P}\Theta_P\right]\left(\overline{U_P} - A\right) \\
&+ \left[\overline{T_{NN}}\,\overline{g}\left(\overline{U_N}\right) + \overline{T_{NP}}\,\overline{g}\left(\overline{U_P}\right) - \overline{a_N}\Theta_N\right]\left(\overline{U_N} - B\right) \\
&= \left[\overline{T_{PP}}\left\{\overline{g}\left(\overline{U_P}\right) - \overline{g}(A)\right\} + \overline{T_{PN}}\left\{\overline{g}\left(\overline{U_N}\right) - \overline{g}(B)\right\} - \overline{a_P}\left\{\overline{U_P} - A\right\}\right]\left\{\overline{U_P} - A\right\} \\
&+ \left[\overline{T_{NN}}\left\{\overline{g}\left(\overline{U_N}\right) - \overline{g}(B)\right\} + \overline{T_{NP}}\left\{\overline{g}\left(\overline{U_P}\right) - \overline{g}(A)\right\} - \overline{a_N}\left\{\overline{U_N} - B\right\}\right]\left\{\overline{U_N} - B\right\}.
\end{aligned}$$

Since $\overline{g}(\cdot)$ is bounded, if region $\Re$ is large enough, $\frac{d\Re}{dt} < 0$ when $\overline{U_P}(t)$ and $\overline{U_N}(t)$ become large. According to Poincaré-Bendixson theorem [AVK66], if $\left(\overline{U_P}(t), \overline{U_N}(t)\right)$ is a solution of the system such that it exists and stays in $\Re$ for $t \geq t_0$ for some finite t_0, then either

(a) the solution is periodic, or
(b) the solution spirals toward a periodic solution as $t \to \infty$, or
(c) the solution terminates at any one of equilibrium points.

A formal statement of this theorem is given in the Appendix. An alternative mathematical analysis to show the existence of periodic solutions can be found in [Gem82].

Figure 7 shows the phase portrait corresponding to each of the cases above. If we can choose an annular region $\Re'$ which excludes all equilibrium points and assume that among these limit cycles there are no "semi-stable" ones (they are only possible in "non coarse" systems), then if all paths enter the region $\Re'$ as t increases, there is at least one stable limit cycle. On the other hand, if all paths leave the region $\Re'$ as t increases, there exists at least one unstable limit cycle.

We have shown that oscillatory solutions can exist in our model consisting of excitatory and inhibitory neurons. Furthermore, we can use Dulac's criterion [AVK66] to identify the situations where no periodic solution exists. If

$$\begin{aligned}
&\frac{\partial\left[\varrho\left(\overline{U_P}(t), \overline{U_N}(t)\right) f_P\left(\overline{U_P}(t), \overline{U_N}(t)\right)\right]}{\partial \overline{U_P}} + \frac{\partial\left[\varrho\left(\overline{U_P}(t), \overline{U_N}(t)\right) f_N\left(\overline{U_P}(t), \overline{U_N}(t)\right)\right]}{\partial \overline{U_N}} \\
&= \left[\overline{g}'\left(\overline{U_P}(t)\right)\overline{T_{PP}} + \overline{g}'\left(\overline{U_N}(t)\right)\overline{T_{NN}} - (\overline{a_P} + \overline{a_N})\right]\varrho\left(\overline{U_P}(t), \overline{U_N}(t)\right) \\
&+ \frac{\partial \varrho\left(\overline{U_P}(t), \overline{U_N}(t)\right)}{\partial \overline{U_P}} f_P\left(\overline{U_P}(t), \overline{U_N}(t)\right) + \frac{\partial \varrho\left(\overline{U_P}(t), \overline{U_N}(t)\right)}{\partial \overline{U_N}} f_N\left(\overline{U_P}(t), \overline{U_N}(t)\right)
\end{aligned}$$

Figure 7: Phase plot of all three possible solutions.

has the same sign in region $\Re$, there exists no limit cycle in $\Re$ (see Appendix). Here $\varrho\left(\overline{U_P}(t), \overline{U_N}(t)\right)$ is any continuous function with continuous derivatives. Let $\varrho \stackrel{\triangle}{=} 1$. Then,

$$\begin{aligned}
\frac{\partial(\varrho f_{_P})}{\partial \overline{U_P}} + \frac{\partial(\varrho f_{_N})}{\partial \overline{U_N}} &\leq \bar{g}'\left(\overline{U_P}(t)\right)\overline{T_{PP}} - (\overline{a_{_P}} + \overline{a_{_N}}) \\
&\leq \bar{g}'(0)\overline{T_{PP}} - (\overline{a_{_P}} + \overline{a_{_N}}) \\
&= q(\lambda, \eta_{_P})\sqrt{\frac{2}{\pi}}\,\overline{T_{PP}} - (\overline{a_{_P}} + \overline{a_{_N}})\,,
\end{aligned}$$

By Dulac's criterion, we obtain the following lemma.

Lemma 3 *If*

$$q(\lambda, \eta_{_P})\sqrt{\frac{2}{\pi}}\,\overline{T_{PP}} \leq \overline{a_{_P}} + \overline{a_{_N}},$$

then there is no periodic solution for equations (9) and (10) with constant $\overline{T}$'s and $\overline{\Theta}$'s.

This means that the neural system must converge to a fixed point. From Lemma 2, we obtain at most five equilibrium points for this system in general. If any of the conditions in (21) and (22) are not satisfied, these equilibrium points become unstable, and any perturbation from the equilibrium causes the system to oscillate.

5 Oscillation Frequency Estimation

Finding the frequency of oscillation in situations when it occurs, is a natural extension in understanding the aggregate behavior of interacting neuron populations.

However, since such systems are highly nonlinear, finding a simple closed-form solution is difficult. In this section, we derive an expression for the fundamental frequency of oscillation. Simulation results given in Section 6 show this estimate to be quite accurate.

If the system is periodic, the solution to equations (9) and (10) can be approximated by the zeroth and first harmonics of their Fourier series.

$$\left.\begin{array}{rcl} \overline{U_P}(t) & = & \alpha_{_P} + \beta_{_P} \sin\omega t \\ \overline{U_N}(t) & = & \alpha_{_N} + \beta_{_N} \sin(\omega t + \delta) \\ \overline{v_{_P}}(t) & = & \overline{g}(\overline{U_P}(t)) = \alpha'_P + \beta'_P \sin\omega t \\ \overline{v_{_N}}(t) & = & \overline{g}(\overline{U_N}(t)) = \alpha'_N + \beta'_N \sin(\omega t + \delta) \end{array}\right\} \tag{23}$$

Here, ω is the first harmonic frequency and δ is the phase difference between $\overline{U_P}(t)$ and $\overline{U_N}(t)$. Since there is no delay in our model, it is obvious that $\overline{U_P}(t)$ and $\overline{v_{_P}}(t)$ as well as $\overline{U_N}(t)$ and $\overline{v_{_N}}(t)$ have the same phase. Substituting equations (23) into (9) and (10) we obtain

$$\left.\begin{array}{rcl} \beta_{_P}\omega\cos(\omega t) & = & -\overline{a_{_P}}\alpha_{_P} - \overline{a_{_P}}\beta_{_P}\sin\omega t - \overline{a_{_P}}\overline{\Theta_P} \\ & + & \overline{T_{PP}}\alpha'_P + \overline{T_{PP}}\beta'_P \sin\omega t \\ & + & \overline{T_{PN}}\alpha'_N + \overline{T_{PN}}\beta'_N \sin(\omega t + \delta) \\ \beta_{_N}\omega\cos(\omega t + \delta) & = & -\overline{a_{_N}}\alpha_{_N} - \overline{a_{_N}}\beta_{_N}\sin(\omega t + \delta) - \overline{a_{_N}}\overline{\Theta_N} \\ & + & \overline{T_{NN}}\alpha'_N + \overline{T_{NN}}\beta'_N \sin(\omega t + \delta) \\ & + & \overline{T_{NP}}\alpha'_P + \overline{T_{NP}}\beta'_P \sin\omega t \end{array}\right\} \tag{24}$$

For simplicity, let $\lambda = \infty$ i.e. the activation function of an individual neuron be a step function. Eq. (7) can then be written as follows:

$$\bar{v} = \bar{g}(\overline{U}) = \frac{1}{2}\left[1 + \Phi\left(\frac{\overline{U}}{\sqrt{2}\,\eta}\right)\right]$$

where the error function is defined as before. Series representation of the error function is given by

$$\Phi(x) = \frac{2}{\sqrt{\pi}} \sum_{k=1}^{\infty} (-1)^{k-1} \frac{x^{2k-1}}{(2k-1)(k-1)!}.$$

Let $x = p + q\sin\omega t$. Then, the coefficient of the constant term is

$$\frac{2}{\sqrt{\pi}} \sum_{k=1}^{\infty} (-1)^{k-1} \frac{p^{2k-1}}{(2k-1)(k-1)!} = \Phi(p)$$

and the coefficient of $\sin\omega t$ is

$$\frac{2}{\sqrt{\pi}} \sum_{k=1}^{\infty} (-1)^{k-1} \frac{p^{2k-2}q}{(k-1)!} = \frac{2}{\sqrt{\pi}} \left[\sum_{k=0}^{\infty} (-1)^{k} \frac{(p^2)^k}{k!}\right] q = \frac{2}{\sqrt{\pi}} q e^{-p^2}.$$

Taylor's expansion of the function $\Psi(t) \triangleq \Phi(p + q\sin\omega t)$ yields

$$\Psi(t) = \Phi(p) + \frac{2}{\sqrt{\pi}} q e^{-p^2} \sin\omega t + \text{high order terms.}$$

Using this result, the Fourier coefficients of the average outputs and average inputs in equation (23) can be related in the following equations:

$$\left.\begin{aligned} \alpha'_P + \beta'_P \sin\omega t &= \tfrac{1}{2}\left[1 + \Phi\left(\tfrac{\alpha_P}{\sqrt{2}\,\eta_P}\right)\right] + \tfrac{\beta_P}{\sqrt{2\pi}\,\eta_P} e^{\frac{-\alpha_P^2}{2\eta_P^2}} \sin\omega t + \cdots \\ \alpha'_N + \beta'_N \sin(\omega t + \delta) &= \tfrac{1}{2}\left[1 + \Phi\left(\tfrac{\alpha_N}{\sqrt{2}\,\eta_N}\right)\right] + \tfrac{\beta_N}{\sqrt{2\pi}\,\eta_N} e^{\frac{-\alpha_N^2}{2\eta_N^2}} \sin(\omega t + \delta) + \cdots \end{aligned}\right\}. \tag{25}$$

¿From equations (24) and (25), the following relations can be derived by matching the coefficients of $\cos\omega t$, $\sin\omega t$, and the constant term.

$$\begin{aligned} \beta_P \omega &= \overline{T_{PN}}\beta'_N \sin\delta && (26)\\ 0 &= -\overline{a_P}\beta_P + \overline{T_{PP}}\beta'_P + \overline{T_{PN}}\beta'_N \cos\delta && (27)\\ 0 &= -\overline{a_P}\alpha_P - \overline{a_P}\,\overline{\Theta_P} + \overline{T_{PP}}\alpha'_P + \overline{T_{PN}}\alpha'_N && (28)\\ \beta_N \omega \cos\delta &= -\overline{a_N}\beta_N \sin\delta + \overline{T_{NN}}\beta'_N \sin\delta && (29)\\ -\beta_N \omega \sin\delta &= -\overline{a_N}\beta_N \cos\delta + \overline{T_{NN}}\beta'_N \cos\delta + \overline{T_{NP}}\beta'_P && (30)\\ 0 &= -\overline{a_N}\alpha_N - \overline{a_N}\,\overline{\Theta_N} + \overline{T_{NN}}\alpha'_N + \overline{T_{NP}}\alpha'_P && (31)\\ \alpha'_P &= \frac{1}{2}\left[1 + \Phi\left(\frac{\alpha_P}{\sqrt{2}\,\eta_P}\right)\right] && (32)\\ \beta'_P &= \frac{\beta_P}{\sqrt{2\pi}\,\eta_P} \exp\left(-\frac{\alpha_P^2}{2\eta_P^2}\right) && (33)\\ \alpha'_N &= \frac{1}{2}\left[1 + \Phi\left(\frac{\alpha_N}{\sqrt{2}\,\eta_N}\right)\right] && (34)\\ \beta'_N &= \frac{\beta_N}{\sqrt{2\pi}\,\eta_N} \exp\left(-\frac{\alpha_N^2}{2\eta_N^2}\right). && (35) \end{aligned}$$

Using the above equations and some algebraic manipulations, we arrive at the expression below for the frequency of oscillation.

$$\omega = \sqrt{\frac{-\overline{T_{PN}}\,\overline{T_{NP}}}{2\pi\eta_P\eta_N \exp\left(\frac{\alpha_P^2}{2\eta_P^2} + \frac{\alpha_N^2}{2\eta_N^2}\right)} - \frac{\eta_N}{\eta_P}\left[\overline{T_{PP}}\frac{\exp\left(-\frac{\alpha_P^2}{2\eta_P^2}\right)}{\sqrt{2\pi}\,\eta_P} - \overline{a_P}\right]^2} \tag{36}$$

where α_P and α_N can be obtained from

$$-\overline{a_P}\alpha_P + \frac{1}{2}\overline{T_{PP}}\Phi\left(\frac{\alpha_P}{\sqrt{2}\,\eta_P}\right) + \frac{1}{2}\overline{T_{PN}}\Phi\left(\frac{\alpha_N}{\sqrt{2}\,\eta_P}\right)$$

$$= \overline{a_P}\,\overline{\Theta_P} - \frac{1}{2}\overline{T_{PP}} - \frac{1}{2}\overline{T_{PN}} \tag{37}$$

$$-\overline{a_N}\alpha_N + \frac{1}{2}\overline{T_{NN}}\Phi\left(\frac{\alpha_N}{\sqrt{2}\,\eta_N}\right) + \frac{1}{2}\overline{T_{NP}}\Phi\left(\frac{\alpha_P}{\sqrt{2}\,\eta_N}\right)$$

$$= \overline{a_N}\,\overline{\Theta_N} - \frac{1}{2}\overline{T_{NN}} - \frac{1}{2}\overline{T_{NP}}. \tag{38}$$

This first order approximation of the frequency is accurate when the condition given below is satisfied.

$$\overline{a_P}\,\eta_N + \overline{a_N}\,\eta_P = \frac{1}{\sqrt{2\pi}}\left[\frac{\overline{T_{NN}}\,\eta_P}{\eta_N}\exp\left(-\frac{\alpha_N^2}{2\eta_N^2}\right) + \frac{\overline{T_{PP}}\,\eta_N}{\eta_P}\exp\left(-\frac{\alpha_P^2}{2\eta_P^2}\right)\right]. \tag{39}$$

6 Experimental Validation

Simulations were performed to validate the results of the last two sections for $\lambda = \infty$. For this special case, the different types of solutions as given by the stability analysis of Section 4, are experimentally observed. We then show that for a system with periodic solutions, the frequency estimation in Section 5 is fairly accurate.

As stated in Section 4, there exist three types of solutions for equation (9) and (10): periodic, spiral to periodic, and fixed point. Simulation results showing all three solutions are presented in Figure 8, 9, and 10. Each figure consists of six graphs:

1. average excitatory input over time, $\overline{U_P}$
2. average inhibitory input over time, $\overline{U_N}$
3. phase portrait of the average excitatory versus inhibitory input
4. average excitatory output over time, $\overline{v_P}$
5. average inhibitory output over time, $\overline{v_N}$
6. phase portrait of the average excitatory versus inhibitory output.

For the periodic case, the frequency can be approximated by equation (36) in Section 5. To simplify the computation, one of the equilibrium points is set at (0,0). Using equations (9) and (10) under these conditions, we obtain the following relations:

$$\overline{a_P}\,\overline{\Theta_P} - \frac{1}{2}\overline{T_{PP}} - \frac{1}{2}\overline{T_{NN}} = 0 \qquad \text{and}$$

$$\overline{a_N}\,\overline{\Theta_N} - \frac{1}{2}\overline{T_{NN}} - \frac{1}{2}\overline{T_{PP}} = 0$$

It is easy to see that $\alpha_P = 0$ and $\alpha_N = 0$ is one of the solutions for equations (37) and (38). For this case, equation (36) and (39) can be reduced to

$$\omega = \sqrt{\frac{-\overline{T_{PN}}\,\overline{T_{NP}}}{2\pi\eta_P\eta_N} - \frac{\eta_N}{\eta_P}\left(\frac{\overline{T_{PP}}}{\sqrt{2\pi}\,\eta_P} - \overline{a_P}\right)^2} \tag{40}$$

Figure 8: Periodic solution.

Figure 9: Spiral to periodic solution.

Figure 10: Fixed point solution.

$\overline{T_{PP}}$	$\overline{T_{PN}}$	$\overline{T_{NP}}$	$\overline{T_{NN}}$	$\overline{a_{_P}}$	$\overline{a_{_N}}$	$f = \frac{\omega}{2\pi}$	
						Theory	Simulation
5.6	-5.6	1.0	-1.0	1.32	0.5	0.037	0.039
4.0	-6.0	1.4	-2.0	0.7	0.1	0.116	0.107
8.0	-12.0	4.0	-6.0	0.7	0.1	0.190	0.176
10.0	-16.0	5.0	-8.0	0.7	0.1	0.220	0.195
10.8	-10.8	3.0	-3.0	2.8	0.31	0.270	0.273
12.8	-12.8	5.0	-5.0	2.8	0.31	0.351	0.352
30.0	-30.0	25.0	-25.0	1.8	0.11	0.636	0.635
171.8	-171.8	163.0	-163.0	2.5	0.61	1.557	1.660

Table 1: Frequency of Oscillation with $\eta_{_P} = \eta_{_N} = 1$.

$$\overline{a_{_P}}\,\eta_{_N} + \overline{a_{_N}}\,\eta_{_P} = \frac{1}{\sqrt{2\pi}}\left(\frac{\overline{T_{NN}}\,\eta_{_P}}{\eta_{_N}} + \frac{\overline{T_{PP}}\,\eta_{_N}}{\eta_{_P}}\right) \tag{41}$$

Simulations confirm that amplitude, frequency, as well as phase shift can be adjusted by changing the parameters used in equation (9) and (10). A wide range of the frequency of oscillation is obtained by changing the $\overline{T}$s and $\bar{a}$s while setting $\eta_{_P} = \eta_{_N} = 1$. Numerical results from the simulations are compared with theoretical results from equation (40), in Table 1.

7 Conclusion

In this paper, we have applied a macroscopic model of cell assemblies to study the qualitative behavior of a simple system consisting of two interacting groups of excitatory and inhibitory neurons. The theory is not only able to determine the situations which lead to oscillatory behavior, but is also able to give a good estimation for the oscillation frequency for such situations. The oscillations in our system stem from the competitive-cooperative dynamics of the neuron groups similar to those studied by Wilson and Cowan [WC72], without any imposed constructs such as the use of periodic forcing functions or oscillator neurons.

The accuracy of the frequency estimation provides incentive to study more complex systems involving several neuronal groups, as well as more intricate phenomena such as phase locking. We believe that quantitative studies of rhythmic behavior will increase in significance with improved understanding of the role of temporal activities in information organization and processing in the brain.

Appendix

The Poincaré-Bendixson Theorem [AVK66]: Let $\mathcal{R}$ be a closed bounded region consisting of nonsingular points of a 2×2 system $\dot{\mathbf{x}} = \mathbf{X}(\mathbf{x})$ such that some positive half-path $\mathcal{H}$ of the system lies entirely within $\mathcal{R}$. Then either $\mathcal{H}$ is itself a closed path, or it approaches a closed path, or it terminates at an equilibrium point.

Dulac's Criterion [AVK66]: For the system $\dot{x} = X(x, y),\ \dot{y} = Y(x, y)$, there are no closed paths in a simply-connected region in which $\frac{\partial(\varrho X)}{\partial x} + \frac{\partial(\varrho Y)}{\partial y}$ is of one sign, where $\varrho(x, y)$ is any function having continuous first partial derivatives.

References

[AB89] A. Atiya and P. Baldi. Oscillations and synchronizations in neural networks: An exploration of the labeling hypothesis. *International Journal of Neural Systems*, 1:103–124, 1989.

[Ama71] S.I. Amari. Characteristics of randomly connected threshold-element networks and network systems. *Proceedings of the IEEE*, 59:35–47, 1971.

[Ama72] S.I. Amari. Characteristics of random nets of analog neuron-like elements. *IEEE Transactions on Systems, Man, and Cybernetics*, 2:1443–1463, 1972.

[Ama90] S.I. Amari. Mathematical foundations of neurocomputing. *Proceedings of the IEEE*, 78:1443–1463, 1990.

[Ami89] D.J. Amit. *Modeling Brain Function.* Cambridge University Press, 1989.

[AVK66] A.A. Andronov, A.A. Vitt, and S.E. Khaikin. *Theory of Oscillators.* Dover, New York, 1966.

[Bai90] B. Baird. Associative memory in a simple model of oscillating cortex. In D. Touretzky, editor, *Advances in Neural Information Processing Systems -II*, pages 69–75. Morgan Kaufmann, San Mateo, CA, 1990.

[Bow90] J.M. Bower. Reverse engineering the nervous system: an anatomical, physiological and computer based approach. In S. Zornetzer, J. Davis, and C. Lau, editors, *An Introduction to Neural and Electronic Networks*, pages 3–24. Academic Press, 1990.

[CG93] H.-J. Chang and J. Ghosh. Pattern association and pattern reterieval in a continuous neural system. *to appear in Biological Cybernetics*, 1993.

[CGL92] H.-J. Chang, J. Ghosh, and K. Liano. A macroscopic model of neural ensembles : Learning-induced oscillations in a cell assembly. *International Journal of Neural Systems*, 3(2):179–198, 1992.

[Cow67] J.D. Cowan. A mathematical theory of central nervous activity, Ph.D. Thesis. Univ. of London, 1967.

[Ede87] G.M. Edelman. *Neural Darwinism.* New York: Basic Books, 1987.

[GC83] S. Grossberg and M. Cohen. Absolute stability of global pattern formation and parallel memory storage by competitive neural networks. *IEEE Transactions on Systems, Man, and Cybernetics*, 13:815–826, 1983.

[Gem82] S. Geman. Almost sure stable oscillations in a large system of randomly coupled equations. *SIAM Journal on Applied Mathematics*, 42:695–703, 1982.

[GH89] J. Ghosh and K. Hwang. Mapping neural networks onto message-passing multicomputers. *Journal of Parallel and Distributed Computing*, 6:291–330, April, 1989.

[GS89] C.M. Gray and W. Singer. Stimulus-specific neuronal oscillations in orientation columns of cat visual cortex. *Proceedings of the National Academy of Sciences, USA*, 86:1698–1702, 1989.

[Hir89] M. W. Hirsch. Convergent activation dynamics in continuous time networks. *Neural Networks*, 2:331–350, 1989.

[Hop84] J.J. Hopfield. Neurons with graded response have collective computational properties like those of two-state neurons. *Proceedings of the National Academy of Sciences, USA*, 81:3058–3092, 1984.

[KKH90] D. Kammen, C. Koch, and P.J. Holmes. Collective oscillations in the visual cortex. In D. Touretzky, editor, *Advances in Neural Information Processing Systems -II*, pages 77–83. Morgan Kaufmann, San Mateo, CA, 1990.

[KS89] C. Koch and I. Segev. *Methods in Neuronal Modeling, from Synapses to Networks.* MIT Press, 1989.

[Pav73] T. Pavlidis. *Biological Oscillators: Their Mathematical Analysis.* Academic Press, 1973.

[Roz69] L.I. Rozonoer. Random logical nets I, II and III. *Automat. Telemekh.*, 1969.

[Som88] H. Sompolinsky. Statistical mechanics of neural networks. *Physics Today*, pages 70–80, 1988.

[SW90] H.G. Schuster and P. Wagner. A model for neuronal oscillations in the visual cortex. *Biological Cybernetics*, 64:77–82, 1990.

[TMW89] R.D. Traub, R. Miles, and R.K.S. Wong. Model of the origin of rhythmic population oscillations in the hippocampal slice. *Science*, 243:1319–1325, 1989.

[vB86] C. von der Malsburg and E. Bienenstock. Statistical coding and short term synaptic plasticity: A scheme for knowledge representation in the brain. In E. Bienenstock, F. Fogelman, and G. Weisbuch, editors, *Disordered Systems and Biological Organization*, pages 247–272. Springer, 1986.

[vdM88] C. von der Malsburg. Pattern recognition by labeled graph matching. *Neural Networks*, 1:141–148, 1988.

[WC72] H.R. Wilson and J.D. Cowan. Excitatory and inhibitory interactions in localized populations of model neurons. *Biophysical Journal*, 12:1–24, 1972.